



Anomalously-low activation energy of nanoconfined MgCO₃ precipitation

Journal:	<i>ChemComm</i>
Manuscript ID	CC-COM-02-2019-001337.R1
Article Type:	Communication

SCHOLARONE™
Manuscripts

COMMUNICATION

Anomalously-low activation energy of nanoconfined MgCO₃ precipitation†

Received 00th January 20xx,
Accepted 00th January 20xx

Quin R.S. Miller^{ab*}, John P. Kaszuba^{ac}, Herbert T. Schaefer^b, Mark E. Bowden^d, Bernard P. McGrail^e
and Kevin M. Rosso^b

DOI: 10.1039/x0xx00000x

Magnesite (MgCO₃) precipitation within the nanoconfined space of adsorbed H₂O films (~5 monolayers) was determined to have an apparent activation energy of only 36±6 kJ/mol, suggesting that Mg²⁺ under nanoconfinement adopts a hydration configuration that mimics that of aqueous Ca²⁺, at least energetically, if not also specifically in hydration structure.

The continued use of fossil fuels in a climate-responding world requires development of efficient carbon capture and sequestration (CCS) technologies, including permanent storage of CO₂ in geologic formations via *in situ* mineralization.^{1, 2} Current models of mineral carbonation reactions in the subsurface are based on bulk thermodynamic equilibria and reaction kinetics. However, the dominant reactive surface area in many host lithologies (e.g. basalt, sandstone, and shale) often derives from nanoporosity,³⁻⁶ where the properties of fluids and chemical reactivity may differ significantly due to the impact of geometric constraints on molecular structure and speciation. Hence, to accurately predict and gain control over subsurface carbon, carbonation mechanisms and kinetics in these unique settings must be better understood. This avenue of inquiry is also relevant across a variety of environmental and engineering topics, such as sustainable hydrocarbon recovery from nanoporous unconventional reservoirs, and potentially the formation of Mg-carbonate biominerals or hydrocarbon

reservoirs. Indeed, understanding ion transport and desolvation and other nanoconfined processes is vital to the design and optimization of functional nanomaterials⁷, catalysts^{8, 9} and energy storage materials.¹⁰⁻¹²

In this study, we determined the kinetics of magnesite precipitation in nanoscale (~1 nm)¹³ interfacial water films by conducting *in operando* X-ray diffraction (XRD) experiments at 90 and 65 °C, using previously-reported procedures (Fig. S1 and Fig. S2).^{14, 15} Synthetic Mg-silicate (forsterite, Mg₂SiO₄) nanoparticles were reacted with water-saturated supercritical CO₂ at 9.0 MPa, which because of the hydrophilicity of the forsterite (and nascent magnesite^{14, 16}) surfaces induce formation of nanoscale interfacial water films. When added to a previously-reported 50 °C dataset at equivalent conditions¹⁴, Arrhenius fits to the temperature dependence revealed a systematic trend with an apparent activation energy of precipitation (AAEP) for magnesite in nanoconfinement that is much lower than expected from bulk system kinetics. The result enables new insights into the hydration kinetics and configurations of nanoconfined Mg²⁺ cations, and suggests that carbonation in nanoconfinement could have faster kinetics than expectations based on bulk kinetics.

Specifically, it is notoriously difficult to produce anhydrous Mg-carbonates at low temperatures (~<65 °C) due to the large amount of energy needed to dehydrate Mg²⁺, as it tightly binds six inner sphere waters.¹⁷⁻¹⁹ The associated sluggish water exchange rate creates a high activation energy for the ligand exchange reactions that enable formation of Mg-O(-C) bonds and crystallization of magnesite. For example, previous bulk crystallization experiments (Table S1) show that the AAEP of CaCO₃ (calcite) is ~44 kJ/mol whereas for magnesite it is ~103 kJ/mol. This difference may be attributed to the 53.6 kJ/mol difference in relative hydration energetics of Mg²⁺ and Ca²⁺, as presciently suggested by Lippmann¹⁸. Although low-temperature (<40 °C)¹⁹⁻²¹ magnesite synthesis has been reported, this study marks the first time a <90 °C magnesite precipitation kinetics have been determined (Table S1).

^a Department of Geology and Geophysics, 1000 E. University Avenue, University of Wyoming, Laramie, WY 82071, USA

^b Physical and Computational Sciences Directorate, Pacific Northwest National Laboratory, P. O. Box 999, MS K8-98, Richland, WA 99352, USA

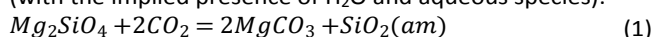
^c School of Energy Resources, 1000 E. University Avenue, University of Wyoming, Laramie, WY 82071, USA

^d William R. Wiley Environmental Molecular Sciences Laboratory, Pacific Northwest National Laboratory, P. O. Box 999, MS K8-98, Richland, WA 99352, USA

^e Energy and Environment Directorate, Pacific Northwest National Laboratory, P. O. Box 999, MS K8-98, Richland, WA 99352, USA

† Electronic Supplementary Information (ESI) available: Experimental materials and methods, Figure S1-S4, Tables S1 and S2. Tabulated apparent activation energies of MgCO₃ and CaCO₃, tabulated experimental results, *in operando* time-resolved XRD figures, *ex situ* thermogravimetric-mass spectrometry measurements, correlated magnesite precipitation rate constants and calculated water exchange rates. See DOI: 10.1039/x0xx00000x

The overall carbonation reaction for MgCO_3 precipitation is (with the implied presence of H_2O and aqueous species):



In the absence of a passivating Si-rich layer on forsterite, magnesite precipitation is the rate-limiting process for this reaction.¹⁴

Here, magnesite precipitation kinetics were quantified at 9.0 MPa with an *in operando* powder XRD technique optimized to interrogate reactions taking place in $\sim 1 \text{ nm}^{13}$ (~ 5 monolayers) H_2O films at the CO_2 - H_2O -mineral interface, environments that facilitate carbonic acid equilibria^{13, 22} and subsequent silicate mineral dissolution^{14, 15, 23, 24}. By fitting time-resolved mineral abundances (Fig. 1) to a first order growth model, 90 °C magnesite precipitation rate constants (k_{Mgs}) were calculated to be 2.9×10^{-5} ($\pm 14\%$) and 2.6×10^{-5} ($\pm 12\%$) s^{-1} (Table S2). The 65 °C and 50 °C k_{Mgs} values were calculated to be 1.1×10^{-5} ($\pm 23\%$) and 6.5×10^{-6} ($\pm 12\%$), respectively. The k_{Mgs} values correlated well with calculated water exchange rates around aqueous magnesium cations (Fig. S3). Carbonation reaction extents, when corrected for co-precipitated amorphous silica¹⁴ (Reaction 1), were in agreement with *ex situ* thermogravimetric-mass spectrometry measurements (Fig. S4).

A least-squares fit of the Arrhenius expression to the rate constants exhibited a regression coefficient of >0.99 , yielding an apparent activation energy of 36 ± 6 kJ/mol for magnesite

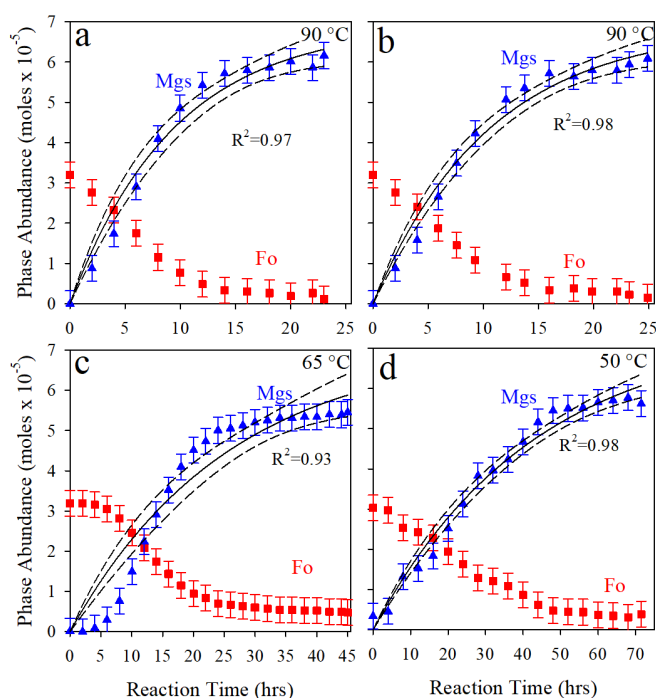


Fig. 1. Quantitative *in operando* X-ray diffraction results. Panels A-D show the time-resolved absolute mineral abundances (moles) for forsterite (Fo, red squares), and magnesite (Mgs, blue triangles). Panel D shows the new kinetic fit to magnesite precipitation temporal trends determined by Miller et al.¹⁴. Black solid lines denote the fit of the magnesite precipitation kinetic model. The coefficients of determination (R^2) for the model are given, and the dashed black lines indicate the 95% confidence intervals.

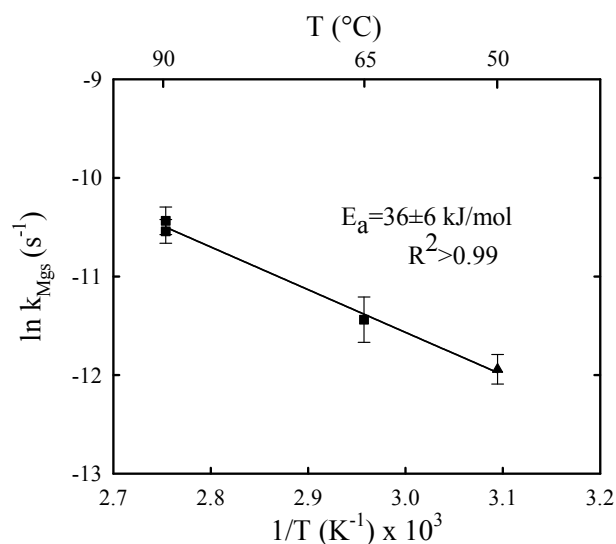


Fig. 2. The variation of the natural logarithm of the *in operando* XRD-determined magnesite precipitation rate constants (k_{Mgs}) as a function of 1000 times the reciprocal absolute temperature (T) of the experiments. Temperature (°C) is labelled on the upper x-axis for reference. The calculated apparent activation energy of magnesite precipitation (50-90 °C and 9.0 MPa), along with the uncertainty, is given next to the trend line.

precipitation in $\sim 1 \text{ nm}$ H_2O films from 50-90 °C (Fig. 2). This value is in close registry with the ~ 44 kJ/mol bulk system AAEP of calcite (Table S1). This drop in the AAEP of magnesite precipitation when nanoconfined suggests that the nominally large dehydration barrier for Mg^{2+} is substantially reduced in the thin water film, rendering the high AAEP of bulk magnesite irrelevant. At the molecular-scale, the similar AAEP values for nanoconfined Mg^{2+} and bulk Ca^{2+} suggest that nanoconfined Mg^{2+} may adopt a hydration configuration that mimics that of aqueous Ca^{2+} , at least energetically, if not also specifically in hydration structure.

More specifically, the reduction in magnesite AAEP is likely due to properties of the virtually two-dimensional reaction environment. Nanoscale water films on mineral surfaces are often highly structured²² and may have dielectric constants up to an order of magnitude less than those of a bulk water (~ 80), sometimes decreasing to single digits in the first few monolayers of adsorbed water²⁵. Increased structuring of water limits the ability of water to reorient and solvate ions, encouraging cation dehydration^{15, 26-28}. A similar lack of water conformational degrees of freedom arises in low-water hypersaline environments, in which natural magnesite precipitation is known to occur^{15, 18}. The greater salinity and reduced water activity in this natural analogue system likely leads to a greater proportion of less-strongly hydrated Mg^{2+} cations, lowering the barrier of cation desolvation and precipitation of magnesite, just like in the $\sim 1 \text{ nm}$ adsorbed water films. We suggest that nanoconfined Mg^{2+} is coordinated by fewer than six inner sphere waters, consistent with other

studies that indicate reductions in coordinating waters around confined ions.²⁸⁻³⁰

In conclusion, experimentally-determined magnesite precipitation kinetics in nanoscale water films are fundamentally faster than those in bulk aqueous fluids. The measurements are strongly suggestive of the key role of Mg²⁺ hydration energetics. The results provide insight into phenomena that are likely relevant across a range of engineered and natural nanoscale environments relevant to sustainable low-carbon energy production. The new knowledge may aid the development of strategies to enhance permanent storage of anthropogenic carbon and help mitigate emissions associated with energy-intense industries. Delineating the dependence of reaction kinetics on the degree of nanoconfinement, the specific hydration structure of nanoconfined ions, and further validating mechanistic interpretations with molecular dynamics simulations are the subjects of our ongoing work.

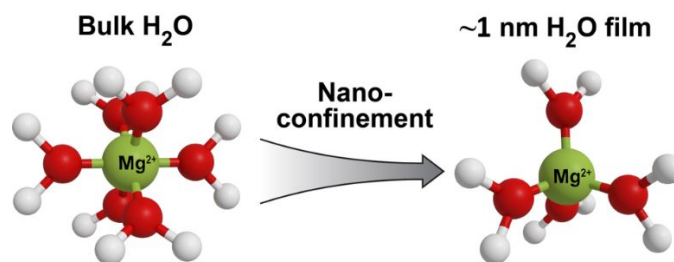
This material is based on work supported by the U.S. Department of Energy (DOE), Office of Science, Office of Basic Energy Sciences (BES), Chemical Sciences, Geosciences, and Biosciences Division through its Geosciences program at Pacific Northwest National Laboratory (PNNL). This BES program supported the activities of QRSM and KMR. A portion of this work was supported by the U.S. Department of Energy Office of Fossil Energy at PNNL through the National Energy Technology Laboratory, Morgantown, West Virginia. QRSM acknowledges initial support by the University of Wyoming (UW) Department of Geology and Geophysics and School of Energy Resources. JPK was supported by the University of Wyoming School of Energy Resources and a Nielson Energy Fellowship. A portion of this work was performed at the Environmental and Molecular Sciences Laboratory (EMSL), a national scientific user facility at PNNL that is managed by the DOE's Office of Biological and Environmental Research. Furthermore, we would like to thank Michael Perkins for graphics support and the input of two anonymous reviewers which helped improve the manuscript.

Conflicts of interest

There are no conflicts to declare.

Notes and references

1. B. P. McGrail, H. T. Schaeff, F. A. Spane, J. B. Cliff, O. Qafoku, J. A. Horner, C. J. Thompson, A. T. Owen and C. E. Sullivan, *Environ. Sci. & Technol. Lett.*, 2017, **4**, 6-10.
2. J. M. Matter, M. Stute, S. O. Snaebjornsdottir, E. H. Oelkers, S. R. Gislason, E. S. Aradottir, B. Sigfusson, I. Gunnarsson, H. Sigurdardottir, E. Gunnlaugsson, G. Axelsson, H. A. Alfredsson, D. Wolff-Boenisch, K. Mesfin, D. F. de la Reguera Taya, J. Hall, K. Dideriksen and W. S. Broecker, *Science*, 2016, **352**, 1312-1314.
3. A. J. Luhmann, B. M. Tutolo, B. C. Bagley, D. F. R. Mildner, W. E. Seyfried and M. O. Saar, *Water Resour. Res.*, 2017, **53**, 1908-1927.
4. I. C. Bourg, L. E. Beckingham and D. J. DePaolo, *Environ. Sci. Technol.*, 2015, **49**, 10265-10284.
5. K. M. Mouzakis, A. K. Navarre-Sitchler, G. Rother, J. L. Bañuelos, X. Wang, J. P. Kaszuba, J. E. Heath, Q. R. S. Miller, V. Alvarado and J. E. McCray, *Environ. Eng. Sci.*, 2016, **33**, 725-735.
6. J. Zachara, S. Brantley, J. Chorover, R. Ewing, S. Kerisit, C. X. Liu, E. Perfect, G. Rother and A. G. Stack, *Environ. Sci. Technol.*, 2016, **50**, 2811-2829.
7. Y. Hu, A. Braganca, L. Verstraete, O. Ivasenko, B. Hirsch, K. Tahara, Y. Tobe and S. J. C. C. De Feyter, *Chem. Commun.*, 2019.
8. S. A. Miners, G. A. Rance and A. N. Khlobystov, *Chem. Soc. Rev.*, 2016, **45**, 4727-4746.
9. C. Zhang, W. Zhu, S. Li, G. Wu, X. Ma, X. Wang and J. Gong, *Chem. Commun.*, 2013, **49**, 9383-9385.
10. V. Augustyn and Y. Gogotsi, *Joule*, 2017, **1**, 443-452.
11. T. Yu, Q. Li, X. Zhao, H. Xia, L. Ma, J. Wang, Y. S. Meng and X. Shen, *ACS Energy Lett.*, 2017, **2**, 2341-2348.
12. J. Sun, D. Li, Y. Xia, X. Zhu, L. Zong, Q. Ji, Y. A. Jia and D. Yang, *Chem. Commun.*, 2015, **51**, 16267-16270.
13. Q. R. S. Miller, D. A. Dixon, S. D. Burton, E. D. Walter, D. W. Hoyt, A. S. McNeill, J. D. Moon, K. S. Thanthiriwatte, E. S. Ilton, O. Qafoku, C. J. Thompson, H. T. Schaeff, K. M. Rosso and J. S. Loring, *J. Phys. Chem. C*, 2019, DOI: 10.1021/acs.jpcc.9b02215.
14. Q. R. S. Miller, H. T. Schaeff, J. P. Kaszuba, L. Qiu, M. E. Bowden and B. P. McGrail, *Environ. Sci. Technol.*, 2018, **52**, 7138-7148.
15. Q. R. S. Miller, J. P. Kaszuba, H. T. Schaeff, M. E. Bowden and B. P. McGrail, *Environ. Sci. Technol.*, 2015, **49**, 4724-4734.
16. J. S. Loring, Q. R. S. Miller, H. T. Schaeff and C. J. Thompson, in *Science of Carbon Storage in Deep Saline Formations: Process Coupling across Time and Spatial Scales*, eds. P. Newell and A. G. Ilgen, Elsevier, 1st edn., 2018.
17. M. Pavlov, P. E. Siegbahn and M. Sandström, *J. Phys. Chem. A*, 1998, **102**, 219-228.
18. F. Lippmann, *Sedimentary Carbonate Minerals*, Springer Berlin Heidelberg, Berlin, Heidelberg, 1973.
19. I. M. Power, P. A. Kenward, G. M. Dipple and M. Raudsepp, *Cryst. Growth Des.*, 2017, **17**, 5652-5659.
20. A. R. Felmy, O. Qafoku, B. W. Arey, J. Z. Hu, M. Hu, H. T. Schaeff, E. S. Ilton, N. J. Hess, C. I. Pearce, J. Feng and K. M. Rosso, *Geochim. Cosmochim. Acta*, 2012, **91**, 271-282.
21. J. C. Deelman, *Neu. Jb. Mineral Mh.*, 1999, 289-302.
22. Q. R. S. Miller, E. S. Ilton, O. Qafoku, D. A. Dixon, M. Vasiliu, C. J. Thompson, H. T. Schaeff, K. M. Rosso and J. S. Loring, *J. Phys. Chem. Lett.*, 2018, **9**, 4988-4994.
23. Q. R. S. Miller, C. J. Thompson, J. S. Loring, C. F. Windisch, M. E. Bowden, D. W. Hoyt, J. Z. Hu, B. W. Arey, K. M. Rosso and H. T. Schaeff, *Int. J. Greenhouse Gas Control*, 2013, **15**, 104-118.
24. H. T. Schaeff, B. P. McGrail, J. L. Loring, M. E. Bowden, B. W. Arey and K. M. Rosso, *Environ. Sci. Technol.*, 2013, **47**, 174-181.
25. L. Fumagalli, A. Esfandiari, R. Fabregas, S. Hu, P. Ares, A. Janardanan, Q. Yang, B. Radha, T. Taniguchi and K. Watanabe, *Science*, 2018, **360**, 1339-1342.
26. Y. F. Wang, C. Bryan, H. F. Xu and H. Z. Gao, *Geology*, 2003, **31**, 387-390.
27. S. Senapati and A. Chandra, *J. Phys. Chem. B.*, 2001, **105**, 5106-5109.
28. R. K. Kalluri, D. Konatham and A. Striolo, *J. Phys. Chem. C*, 2011, **115**, 13786-13795.
29. J. Nelson, J. R. Bargar, L. Wasylenki, G. E. Brown and K. Maher, *Geochim. Cosmochim. Acta*, 2018, **240**, 80-97.
30. Y. Diao and R. M. Espinosa-Marzal, *PNAS*, 2016, **113**, 12047-12052.



Experimental study of nanoconfined $MgCO_3$ nucleation and growth processes reveal elevated kinetics due to less strongly hydrated Mg^{2+}